ChemSusChem

Research Article
doi.org/10.1002/cssc.202400440

Chemistry Europe
European Chemical Societies Publishing

www.chemsuschem.org

Cathodic Conversion of Pressurized CO_2 at Silver Cathodes: What are the Optimal Values of Pressure and Current Density?

Federica Proietto,*[a] Giuseppe Cammisa,[a] Mario Contino,[a] Rosalinda Inguanta,[a] Alessandro Galia,[a] and Onofrio Scialdone*[a]

The cathodic reduction of pressurized CO_2 ($PrCO_2CR$) at suitable cathodes can allow to produce various chemicals, such as formic acid/formate (FA) and carbon monoxide or synthesis gas, with high faradic efficiencies (FEs) and productivities. Here, we have performed the conversion of CO_2 in an undivided pressurized electrochemical reactor using silver cathode in order to determine the optimal values of CO_2 pressure and current density. It was found that the plot FE vs. pressure resulted in a curve with a maximum. Similarly, an optimal value of current density can be selected for the $PrCO_2CR$. The competition between the production of carbon monoxide and formic acid/formate is strongly affected by both the pressure and the current density. Eventually the effect of pressure and current density on the economic figures of the process was evaluated.

1. Introduction

Cathodic reduction of CO_2 (CO_2CR) to various chemicals is considered a very promising route to upgrade/use captured CO_2.[1–9] CO_2CR can be used to synthesize carbon monoxide (CO), formate/formic acid, synthesis gas, alcohols, and hydrocarbons. Moreover, CO_2CR can benefit from the utilization of renewable electricity. Most studies have been focused on the utilization of advanced cathodes or of gas diffusion electrodes at atmospheric CO_2 pressure.[1–9] However, the utilization of pressurized CO_2 is appealing for CO_2CR for many reasons:

- CO_2 in various exhaust streams from power and industrial sources is present in pressurized conditions (1–20 atm);[10]
- the use of pressurized CO_2 increases its solubility in aqueous solutions, thus accelerating the steps involved in its cathodic transformation and increasing the productivity of the electrochemical cell, and, on overall, improving the process from an economic point of view;[11–13]
- some products of CO_2CR, such as CO and syngas, are used for some applications under pressurized conditions;[14,15]
- it allows to use cheap and simpler cathodes, such as tin plates.[12]

At 1 bar and using plate cathodes, the low CO_2 solubility gives rise to low limiting current densities (j_{lim}) for the CO_2 mass transport to the cathodic surface close to 30 mA cm^{-2},[5] thus resulting in low productivities. The utilization of pressurized CO_2 gives rise to relevant solubilities of CO_2 and decrease the bulk catholyte pH: in water solutions, at 25 °C, a pressure increases from 1 to 10 and 50 bar gives rise to CO_2 concentrations close to 33 mM, 0.31 M and 1.31 M, respectively.[16] More in general, the use of pressurized CO_2 has been reported to increase the selectivity of CO_2CR and partial current densities towards CO_2 reduction products.[17–21] Moreover, pressurizing may favor the integration of the CO_2CR with upstream and downstream operations. The cathodic reduction of pressurized CO_2 ($PrCO_2CR$) was studied at various cathodes.[17–35] In 1993–1995, the works of Sakata and co-authors showed that the usage of pressurized CO_2 allows to significantly enhance the production of CO and formic acid/formate (FA) using many electrodes[22–25] and to decrease the generation of hydrogen. Moreover, it was recently highlighted that, for pressurized conditions, the morphology and the porosity of the electrode seem to affect in a less relevant way the figures of merit of the process.[17,18] Most of the works on $PrCO_2CR$ were focused to the production of CO using silver[18–20] and of FA using tin cathodes;[21,26–29] even if also other electrodes were successfully tested including In, Pb, Cu, Au, etc..[24,30–33,36–38] As an example, Lamaison et al.[36] reported a drastic increase of the CO partial current density to −286 mA cm^{-2} at a CO_2 pressure of 9.5 atm on an Ag–Zn alloy dendrite. Theoretical models were also developed to understand $PrCO_2CR$.[39,40] Some authors reported a complex effect of pressure (P) and of current density (j). It was found that the plot faradic efficiency in products generated by CO_2 reduction (FE_{CO2_TOT}) vs. the P give a monotonic increase with the pressure at Pb (for P between 1 and 50 bar in 0.2 M K_2CO_3 aqueous electrolyte for potentiostatic electrolyses[31]), but a plateau value for Sn (for P between 20 and 30 bar with 0.1 M Na_2SO_4 at

[a] Dr. F. Proietto, G. Cammisa, M. Contino, Prof. R. Inguanta, Prof. A. Galia, Prof. O. Scialdone
Dipartimento di Ingegneria
University of Palermo
Viale delle Scienze, Ed. 6, 90128, Palermo, Italy
E-mail: federica.proietto@unipa.it
onofrio.scialdone@unipa.it

Supporting information for this article is available on the WWW under https://doi.org/10.1002/cssc.202400440

pH 4[27] and at around 40 bar in 0.5 M $KHCO_3$ aqueous electrolyte[21]) or even a maximum at Cu cathodes for P of 50 bar and j of -163 mA cm^{-2} with 0.1 M $KHCO_3$ as supporting electrolyte (SE).[23] In some cases, a maximum in the plot FE_{CO2_TOT} vs. j was reported.[26] Moreover, it was found that the effect of the P can strongly depend on the adopted j[26] and that the P affects the selectivity of the CO_2 reduction.[23,25,32]

From an applicative point of view, the optimization of the process requires the selection of the optimal values of both CO_2 pressure (P_{CO2}) and j, with the aim of improving the *i*) faradic efficiency (FE) in the target products, thus leading to the reduction of the energetic consumptions (EC), *ii*) the productivity of the cell, thus reducing the impact of the capital costs, and *iii*) the stability, thus reducing the impact of the cost of electrodes, without excessive values of the cell potential (ΔV). In our previous work on $PrCO_2CR$,[18] we investigated the effect of the pressure (limits to 1, 15, 20, 30 bar) using Ag-based cathodes (plate Ag and high surface Ag electrode) changing the nature of the SE (K_2SO_4, KCl, KOH, $KHCO_3$) and at relatively low j values (-12, -36 and -50 mA cm^{-2}), which, according to recent literature,[12] are not suitable for the commercialization of this technology. The common finding of this work was that the use of pressurized condition is a viable way to increase the productivity in CO (r_{CO}) and reduce the cell (ΔV) at low j values. However, the reached performances, such as the r_{CO}, were not suitable to meet the requirement of the applicative scale since, for the economic feasibility, the process should reach simultaneously high j (>100 mA cm^{-2}), high FE, low EC as well as stability with the time. Hence, with the aim to find the optimum j and P values, we have decided to evaluate in detail the coupled effect of j at high values (ranged from -50 to -230 mA cm^{-2}) and of P_{CO2} (1, 5, 15, 30, 40, 50 bar) on $PrCO_2CR$ in aqueous electrolyte using a Ag cathode and $KHCO_3$ as SE on a large set of key process parameters. These parameters include the FE in the main products, the EC and the productivity (r). Moreover, a comparison from an economical point of view of most interesting adopted operative conditions was performed.

2. Results and Discussion

2.1. Effect of the Pressure at Various Current Densities at Ag Cathode

First electrolyses were carried out at -50 mA cm^{-2} for 120 min using a Ti/IrO_2-Ta_2O_5 anode and an Ag cathode with magnetic stirring (500 rpm). 0.5 M $KHCO_3$ was used as a SE since this SE is largely used in literature for the CO_2CR at various cathodes and since it was reported to favor both the CO_2CR and $PrCO_2CR$ at Ag cathodes.[18] The effect of P_{CO2} was evaluated changing P_{CO2} from 1 to 50 bar. First experiments were carried out at 5 bar. The CO_2CR gave rise to the formation of CO (FE_{CO} 52%) and formate (FE_{FA} 11%) (Figure 1A, primary y-axis) for a selectivity in CO (S_{CO}) close to 83% (Figure 1A, secondary y-axis). Moreover, hydrogen was produced by cathodic reduction of water with a FE (FE_{H2}) slightly lower than 40%. The overall FE in the products generated by the CO_2CR ($FE_{CO2\_TOT} = FE_{CO} + FE_{FA}$) was close to 63%, the overall productivity (r_{TOT}) to 1.6 mmol$_{TOT}$ s^{-1} m^{-2}, the ΔV to 3.9 V and the EC to 0.33 kWh mol$_{TOT}^{-1}$ (Figure 1B, secondary y-axis). To highlight the role on the effect of relatively high-pressure of CO_2 to the performances of the process, reference electrolysis was performed at atmospheric pressure of CO_2. As showed in Figure 1A, the cathodic reduction of CO_2 was likely to be limited by the decreasing of pressure from 5 to 1 bar reducing the FE_{CO2_TOT} from 63 to 15%, respectively, in favor of the hydrogen evolution ($FE_{H2} \sim 85\%$).

When P_{CO2} was increased to 15 and 30 bar (Figure 1A, primary y-axis), CO_2 reduction was strongly favored (FE_{CO2_TOT} of 63, 69 and 90% at 5, 15 and 30 bar, respectively). Conversely, the FE_{H2} was reduced and at 30 bar it was slightly lower than 25%. However, a further increase of the P_{CO2} to 40 and 50 bar resulted in a decrease of FE_{CO2_TOT} to 75 and 70%, respectively. Also, the FE_{CO} presented, as FE_{CO2_TOT}, a curve with a maximum with the P_{CO2} while FE_{FA} decreased with P_{CO2} (Figure 1A). Indeed at 1, 5, 15, 30 bar, FE_{CO} was 3, 52, 60 and 83% and FE_{FA} 12, 11, 9 and 7%, respectively, while the further increase of the P to 40 and 50 bar resulted in a decrease of both FE_{CO} (70 and 67%, respectively) and FE_{FA} (5 and 3%, respectively) and in the consequent increase of the hydrogen production. Consequently, the increase of P_{CO2} from 1 to 50 bar resulted in a significant increase of S_{CO} from 20 to 95% (Figure 1A, secondary y-axis). Figure 1B reports the effect of the P_{CO2} on ΔV and EC. It is interesting to observe that the P increases resulted in a slight reduction of ΔV (refers also to the chronoamperometric curves reported in Figure S1 of the Supporting Information), probably due to the enhanced CO_2 mass transfer and adsorption kinetics which leads to less negative working potentials, while the plot EC vs. P_{CO2} resulted in a curve with a minimum of 0.23 kWh mol$_{TOT}^{-1}$ for a P of 30 bar. Indeed, EC depends linearly on ΔV (which slightly reduced with P_{CO2}) and it is inversely proportionally on FE_{CO2_TOT} which presented a maximum for 30 bar.

Some authors, in previous studies, studied the effect of the P on the CO_2CR using Ag based cathodes[18–20,32] for P between 1–30 bar, founding that the increase of P_{CO2} results in an enhancement of both FE_{CO2_TOT} and FE_{CO}. Moreover, Gabardo and coauthors[19] reported a reduction of FE_{FA} with P_{CO2} at Ag-GDE; conversely, Huang and coauthors[32] reported a strong increase of FE_{FA} with the pressure at -1.1 V vs. RHE using Ag based cathodes using 0.5 M $KHCO_3$ aqueous solutions. However, for this last work, the use of a fixed working potential resulted in a very strong change of j from approximately -40 to -80 mA cm^{-2}.[32]

According to the literature, the increase of P_{CO2} leads to a higher CO_2 surface coverage, and therefore to a probable reduction in the protons adsorbed number on the surface of the catalyst, thus favoring the reduction of CO_2 with respect to the hydrogen evolution.[19] To explain the adverse effect of P_{CO2} on FE_{CO2_TOT} observed for the highest values of the P different factors should be taken in account:

- the increase of P_{CO2} leads to a decrease of pH, thus increasing the concentration of protons in the bulk; indeed, in 0.5 M $KHCO_3$, the increase of P_{CO2} from 1 to 60 bar is expected to decrease the pH from about 7.5 to 6,[21,41] and, according to

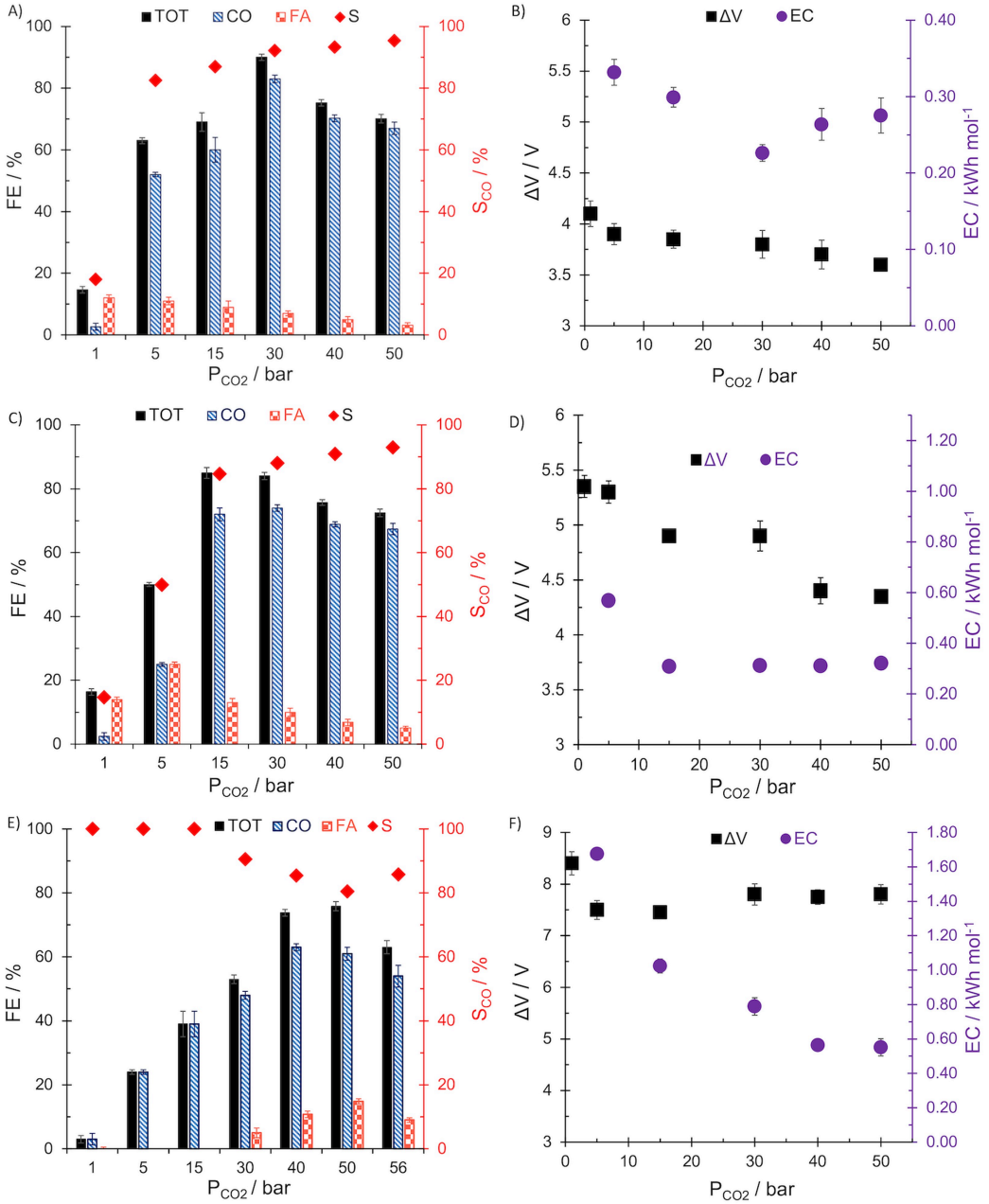

Figure 1. Effect of the P (1 ÷ 56 bar) on the CO_2CR process at different *j* (−50, −90 and −190 mA cm^{-2}) values. Plot of (A) FE_{CO2_TOT}, FE_{CO} and FF_{FA} (primary y-axis) and S_{CO} (secondary y-axis) and relative (B) ΔV (primary y- axis) and EC (secondary y-axis) at −50 mA cm^{-2}. Plot of (C) FE_{CO2_TOT}, FE_{CO} and FE_{FA} (primary y-axis) and S_{CO} (secondary y-axis) and relative (D) ΔV (primary y- axis) and EC (secondary y-axis) at −90 mA cm^{-2}. Plot of (E) FE_{CO2_TOT}, FE_{CO} and FE_{FA} (primary y-axis) and S_{CO} (secondary y-axis) and (F) relative ΔV (primary y- axis) and EC (secondary y-axis) at −190 mA cm^{-2}. EC at 1 bar was estimated of 1.50, 1.64, 15 kWh mol$_{TOT}^{-1}$ at −50, −90 and −190 mA cm^{-2}, respectively (data not showed in 1B, 1D and 1F, respectively). Electrolyses were performed in a CO_2-saturated 0.5 M $KHCO_3$ aqueous electrolyte using Ag cathode and DSA anode for 120 minutes. V = 0.05 L. N = 500 rpm. *Q* = 0.1 L min^{-1}

the literature, the conversion of CO_2 to CO using Ag electrodes is favored increasing the pH;[42]

- for very high P_{CO2}, a very high coverage of the adsorbed intermediates on the Ag surface is expected, thus limiting the impact of further increases of the P on the reduction of CO_2.

To explain the increase of S_{CO} with P_{CO2}, different hypotheses can be done. According to Gabardo et al.,[19] the increase of P_{CO2} leads both to a higher CO_2 surface coverage and to a lower proton one, that can favor the CO production over the FA one,[43] even if other authors reported that a higher CO_2 coverage should favor the formate production.[31]

From an applicative point of view, it would be appealing to operate the electrolysis at higher *j* to enhance the productivity of the cell.

Hence, the effect of the P was evaluated also at −90 and −190 mA cm^{-2}. As shown in Figures 1C and 1E, also in this case the plot FE_{TOT} vs. CO_2 pressure gave a curve with a maximum. In particular, at −90 mA cm^{-2} the maximum FE_{CO2_TOT} was obtained

at 15 and 30 bar and it was close to 85% (Figure 1C), while, at -190 mA cm^{-2}, the maximum was reached at 50 bar and it was close to 76% (Figure 1E). As an example, at -190 mA cm^{-2} and 50 bar, FE_{CO2_TOT} and FE_{H2} were close to 76 and 26%, respectively. Similarly, also at -90 and -190 mA cm^{-2}, FE_{CO} presented a maximum with the P. In particular, at -90 and -190 mA cm^{-2}, the maximum FE_{CO} were 72 and 63%, respectively, and they were achieved at 30 and 40 bar, respectively, (Figures 1C and 1E, respectively). FE_{FA} presented a different trend depending on the value of the *j*. At the lowest *j* of -50 and -90 mA cm^{-2}, FE_{FA} decreased monotonically with the P_{CO2}; as an example, at -90 mA cm^{-2}, FE_{FA} decreased from 25 to 5% increasing the P_{CO2} from 5 to 50 bar (Figure 1C). Conversely, at the highest value of *j* of -190 mA cm^{-2}, FE_{FA} presented a maximum value for P_{CO2} of 50 bar (Figure 1E), thus showing that FA formation depends on both P and *j*. However, S_{CO} decreased with P_{CO2} for all adopted *j* with the exception of the highest values of the P_{CO2} (50 and 56 bar) and *j* (-190 mA cm^{-2}) (Figure 1E).

As shown in Figures 1D and 1F, at both -90 and -190 mA cm^{-2}, the lowest ΔVs were obtained at the highest P_{CO2} while the plot EC vs. P_{CO2} resulted always in a curve with a minimum, that was achieved in the conditions that optimized FE_{CO2_TOT} (between 15 and 30 bar at -90 mA cm^{-2} (Figure 1D) and between 40 and 50 bar at -190 mA cm^{-2} (Figure 1F)).

2.2. Effect of the Current Density at Ag Cathode

The effect of *j* on $PrCO_2CR$ was evaluated carrying out different series of electrolyses changing *j* from -50 to -230 mA cm^{-2} and using different P_{CO2} values (30, 40, and 50 bar). Figures 2A, 2D and 2G report the effect of *j* on the FEs and on S_{CO}. It is clearly shown that at 30 bar, the increase of *j* from -50 to -190 mA cm^{-2} gave rise to a significant reduction of FE_{TOT} from 90 to 53% (Figure 2A, primary y-axis), while S_{CO} presented similar values close to 90% (Figure 2A, secondary y-axis). It is interesting to observe that the j_{lim}, under adopted operative conditions, for a process under the CO_2 mass transfer control to

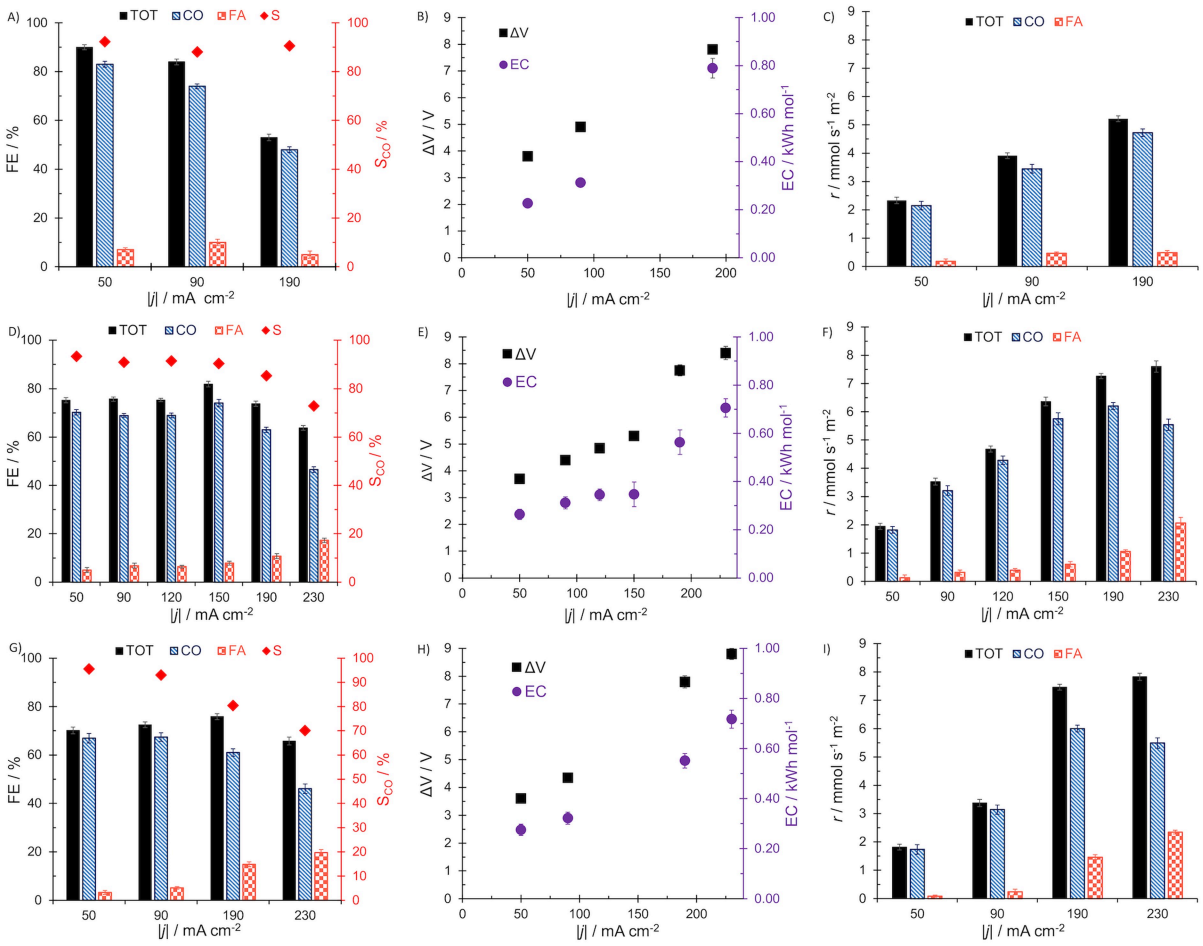

Figure 2. Effect of the *j* ($-50 \div -230$ mA cm^{-2}) on the CO_2CR process at different P values (30, 40 and 50 bar). Plot of (A) FE_{CO2_TOT}, FE_{CO} and FE_{FA} (primary y-axis) and S_{CO} (secondary y-axis), relative (B) ΔV (primary y- axis) and EC (secondary y-axis) and (C) r_{TOT}, r_{CO} and r_{FA} at 30 bar. Plot of (D) FE_{CO2_TOT}, FE_{CO} and FE_{FA} (primary y- axis) and S_{CO} (secondary y-axis), relative (E) ΔV (primary y- axis) and EC (secondary y-axis) and (F) r_{TOT}, r_{CO} and r_{FA} at 40 bar. Plot of (G) FE_{CO2_TOT}, FE_{CO} and FE_{FA} (primary y- axis) and S_{CO} (secondary y-axis), relative (H) ΔV (primary y- axis) and EC (secondary y-axis) and (I) r_{TOT}, r_{CO} and r_{FA} at 50 bar. Electrolyses were performed in a CO_2-saturated 0.5 M $KHCO_3$ aqueous electrolyte using Ag cathode and DSA anode for 120 minutes. V = 0.05 L. N = 500 rpm. $Q = 0.1$ L min^{-1}.

the cathode is close to 500 mA cm^{-2}. Hence, the reduced FE_{TOT_CO2} observed at high *j* cannot be attributed to mass transfer kinetic limitations. In the case of the CO_2CR using tin cathodes, the negative effect of *j* observed at relatively low pressures was related to the fact that high *j* reduces the surface coverage by CO_2, thus favoring the competitive adsorption of H and advancing the hydrogen evolution.[39] When the P_{CO2} was increased to 40 and 50 bar (Figures 2D and 2G, respectively), the effect of *j* on FE_{TOT_CO2} was quite small up to −190 mA cm^{-2}. Indeed, at 40 bar, from −50 to −190 mA cm^{-2}, FE_{TOT_CO2} presented a value between 73 and 81 %, with a maximum value at −150 mA cm^{-2}, but it decreases to 63 % at −230 mA cm^{-2} (Figure 2D). Similarly, at 50 bar, FE_{TOT_CO2} presented a value between 66 and 75 % in the quite large interval −50 ÷ −230 mA cm^{-2} with a maximum value (Figure 2G). Hence, it can be concluded that, for these relatively high values of the P_{CO2}, almost all the adopted *j* can be used with quite good FE_{TOT_CO2}. However, as shown in Figures 2D and 2G, the similar values of FE_{TOT_CO2} observed at different *j* are due to opposite trends of FE_{CO} and FE_{FA}.

Indeed, FE_{CO} decreased with *j* while FE_{FA} presented the opposite trend. Hence, at both 40 and 50 bar, S_{CO} decreased with *j* (Figures 2D and 2G). Similar results were previously reported by Hara et al.[25] on Ag electrode under 30 atm CO_2 in 0.1 M $KHCO_3$.

In order to understand the complex effect of P_{CO2} and *j* on S_{CO}, it could be useful to remember that according to many authors,[44–48] CO, HCOOH and H_2 are likely to be formed in carbonate solutions by the following paths:

Path 1

$$CO_2 + H_2O + e^- + * = COOH_{ad} + OH^- \quad (1)$$

$$COOH_{ad} + H_2O + e^- \rightarrow CO + H_2O + OH^- + * \quad (2)$$

Path 2

$$CO_2 + H_2O + e - + * = HCOO_{ad} + OH^- \quad (3)$$

$$HCOO_{ad} + H_2O + e^- \rightarrow HCOOH + OH^- + * \quad (4)$$

Path 3

$$H_2O + e^- + * = H_{ad} + OH^- \quad (5)$$

$$H_{ad} + H_2O + e^- \rightarrow H_2 + OH^- + * \quad (6)$$

Relatively high P_{CO2} and/or low *j* are expected to give a high coverage of the cathode surface by CO_2 reduction intermediates and a low coverage by H.[44]

Conversely, low P_{CO2} and/or high *j* should lead to higher coverages by H, thus favoring the hydrogen evolution. However, according to Zhang et al.,[36] a higher H-coverage is expected to favor H_2 evolution, but also to stabilize $HCOO_{ad}$, thus enhancing the formic acid/formate formation.[43] Conversely, a low H-coverage is expected to inhibit the H_2 evolution and to favor the formation of $COOH_{ad}$ which is expected to evolve mainly to CO, according to the results above described.

Figures 2B, 2E and 2H report the effect of *j* at 30, 40 and 50 bar, respectively, on ΔV and EC. It is observed that ΔV increased as expected with *j* even if this increase is particularly high for the highest adopted *j* (−190 and −230 mA cm^{-2}) as a probable result of too high ohmic drops caused by the not very high adopted concentration of SE. EC showed a similar increase with *j*. In particular, at all adopted P_{CO2}, EC was close or lower than 0.35 kWh mol_{TOT}^{-1} for *j* up to −150 mA cm^{-2} and higher than 0.70 kWh mol_{TOT}^{-1} for the highest adopted *j* of −230 mA cm^{-2}, as a concomitant effect of the very high ΔV and the lower FE_{CO2_TOT}. If EC is a key parameter to determine the impact on the process of energetic costs, the productivity is a relevant factor that strongly affects the impact on the process of capital costs. Hence, Figures 2C, 2F and 2I report the productivities achieved under the adopted operative conditions. The use of pressurized CO_2 allowed to achieve a strong increase of the total productivity (r_{TOT}) upon increasing *j* at all adopted P_{CO2}, because of the very small decrease of FE_{TOT} observed at high *j*, particularly at 40 and 50 bar (Figures 2F and 2I). Hence, the highest r_{TOT} were obtained at −190 and −230 mA cm^{-2} for all used P (Figures 2C, 2F, 2I). In particular, maximum values of r_{TOT} were between 7.3 and 7.8 mol_{TOT} s^{-1} m^{-2} for *j* between −190 and −230 mA cm^{-2} s^{-1} at both 40 and 50 bar but presented values lower than 5.2 mol_{TOT} s^{-1} m^{-2} at 30 bar because of the reduced values of FE_{TOT} achieved at this lower pressure at high *j*. A different scenario is observed for the productivities in CO (r_{CO}) and formate (r_{FA}):

- for formate, the productivity strongly increased with *j* because of the concomitant effect of the faster CO_2 reduction and of higher S_{FA} achieved at high *j* and presented the maximum values at −230 mA cm^{-2}; as an example, at 50 bar r_{FA} increased from 0.1 to 2.3 mol_{FA} s^{-1} m^{-2} upon increasing *j* from −50 to −230 mA cm^{-2} (Figure 2I);
- for CO, the productivity presented a maximum close to 6 mol_{FA} s^{-1} m^{-2} at both 40 and 50 bar for *j* of −190 mA cm^{-2} (Figures 2F and 2I), because of the positive effect of *j* on FE_{TOT} and its negative effect on S_{CO} which was particularly relevant at high *j* (Figures 2D and 2G).

2.3. Coupled Effect of P_{CO2} and Current Density

Figure 3 reports the coupled effect of P_{CO2} and *j* on the FE and on the *r*. As shown in Figure 3A, in order to optimize FE_{CO2_TOT}, intermediate values of both P_{CO2} and *j* should be selected. Indeed, values of FE_{CO2_TOT} higher than 80 % were achieved at 30 bar at −50 and −90 mA cm^{-2} (90 and 84 %, respectively), at 15 bar and −90 mA cm^{-2} (85 %) and at 40 bar and −150 mA cm^{-2} (82 %). However, it is worth to mention that $PrCO_2$CR at 40 and 50 bar allowed to achieve quite good FE_{CO2_TOT} for a large set of operative conditions (e.g. $FE_{CO2\_TOT} > 70$ % at 40 and 50 bar for *j* from −50 to −190 mA cm^{-2}). Figure 3B

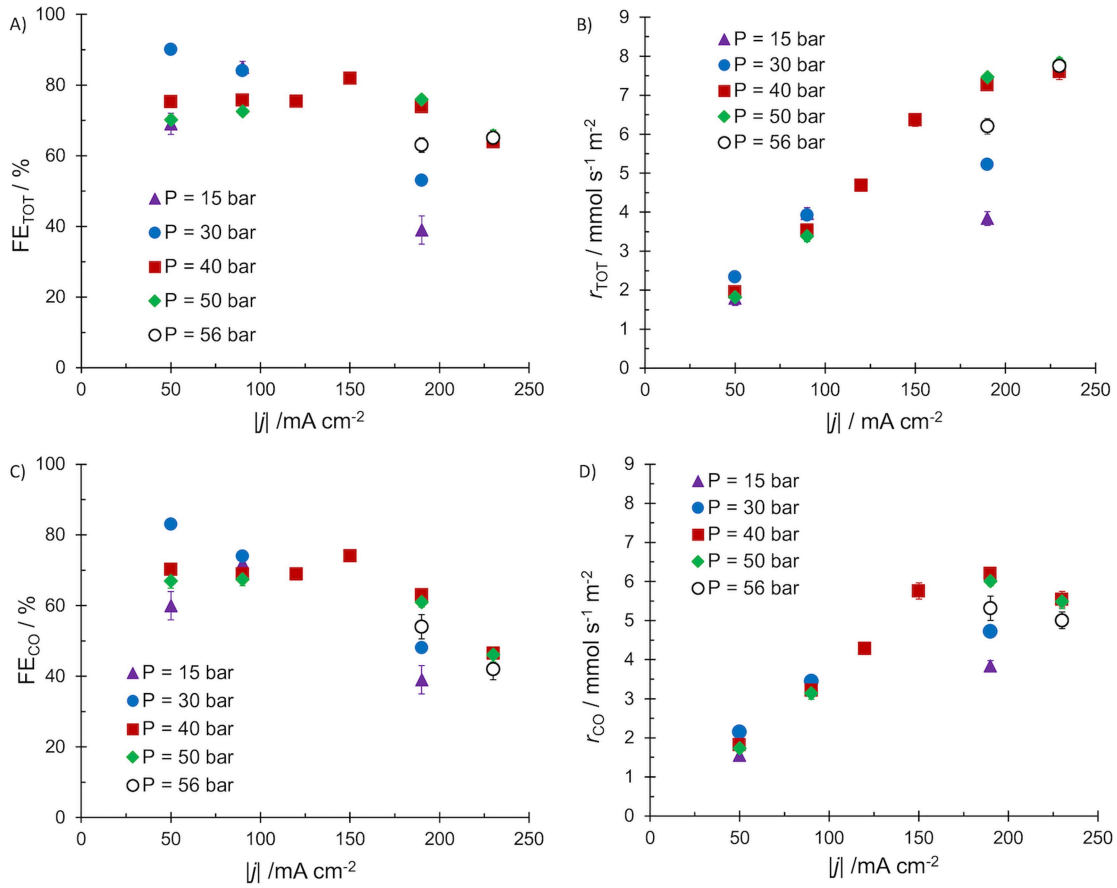

Figure 3. Coupled effect of both P (15 ÷ 56 bar) and j (−50 ÷ −230 mA cm^{-2}) on the CO_2CR process. Plot of (A) FE_{TOT} and (B) r_{TOT} vs. j at fixed P values. Plot of (C) FE_{CO} and (D) r_{CO} vs. j at fixed P values. Electrolyses were performed in a CO_2-saturated 0.5 M $KHCO_3$ aqueous electrolyte using Ag cathode and DSA anode for 120 minutes. V = 0.05 L. N = 500 rpm. Q = 0.1 L min^{-1}.

reports the coupled effect of P_{CO2} and j on the overall productivity in CO and formate (r_{TOT}). The highest productivities, higher than 7 mmol s^{-1} cm^{-2}, were achieved using the highest values of j and quite high P_{CO2}: −190 mA cm^{-2} at 40 and 50 bar and −230 mA cm^{-2} at 40, 50 and 56 bar. These high r were guaranteed by the ability of $PrCO_2CR$ to achieve good FE_{TOT} also at high j. The effect of j and P_{CO2} on the FE_{CO} is described in Figure 3C. The highest FE_{CO} (~83 %) was achieved at −50 mA cm^{-2} and 30 bar. However, quite good FE_{CO} were obtained for various operative conditions. As an example, FE_{CO} > 70 % was achieved at −50 mA cm^{-2} at 30 and 40 bar, at −90 mA cm^{-2} at 15 and 30 bar and at −150 mA cm^{-2} and 40 bar. As shown in Figure 3D, the highest r_{CO} were obtained neither at the j that optimized the FE_{CO} nor at the highest j of −230 mA cm^{-2} but at the intermediate value of j of −190 mA cm^{-2} at 40 and 50 bar.

2.4. Effect of $KHCO_3$ Concentration

Some electrolyses were repeated aiming to evaluate the effect of $KHCO_3$ concentration on FE, r, ΔV and EC and to try to decrease the very large ΔVs observed at high js. Two different j were used to test this aspect: −50 and −190 mA cm^{-2}. For each of these j, the pressure that optimizes the performances of the process was selected according to results reported in Section 2.1. As shown in Table 1, the increase of the SE concentration has both positive and negative effects:

- a decrease of FE_{CO2_TOT} and r_{TOT} was observed, caused by the decrease of FE_{CO} and the increase of FE_{FA} which, however, not compensates completely the decrease of FE_{CO}; e.g., at −50 mA cm^{-2} and 30 bar, FE_{CO2_TOT} was 90 and 68 % using $KHCO_3$ with a concentration of 0.5 and 1 M, respectively, (Table 1, entries 1 and 2);
- a reduction of the required ΔV.

The adverse effect of the concentration of $KHCO_3$ on the $PrCO_2CR$ to CO was previously reported at Cu cathodes.[47] According to these authors, K^+ accumulates nearby the working electrode due to its electro-positivity and at high concentrations inhibiting more the adsorption of CO_2 on the working electrode with respect to that of H^+ since the H^+ dimension is considerably smaller than the K^+ (i.e. 25–50 pm vs. 150–250 pm for H^+ and K^+, respectively).[38] On overall, the increase of $KHCO_3$ resulted in a slight increase of EC, and, as a consequence, did not allow to improve the process performances.

Table 1. Effect of the SE concentration of the performances of the $PrCO_2CR$.[a]

Entry	[$KHCO_3$] (M)	j (mA cm^{-2})	P_{CO2} (bar)	FE_{CO2_TOT} [FE_{CO}; FE_{FA}] (%)	r_{TOT} [r_{CO}; r_{FA}] (mmol s^{-1} cm^{-2})	ΔV (V)	EC (kWh/mol)
1	0.5	−50	30	90 [83; 7]	2.4 [2.2; 0.2]	3.8	0.23
2	1.0	−50	30	68 [53; 15]	1.8 [1.4; 0.4]	3.5	0.28
3	0.5	−190	50	76 [61; 15]	7.5 [6.0; 1.5]	7.8	0.55
4	0.75	−190	50	63 [36.5; 26.5]	6.2 [3.6; 2.6]	6.6	0.56
5	1	−190	50	36 [23; 13]	3.5 [2.2; 1.3]	6.3	0.95

[a] Electrolysis were performed for 120 min at 500 rpm using Ag and DSA as cathode and anode, respectively. Volumetric gas flow (Q) of 0.1 L min^{-1}.

2.5. Effect of Pressure and Current Density on Economic Figures of the $PrCO_2CR$

The main economic figures of the $PrCO_2CR$ using Ag cathode were evaluated at various operative conditions under the assumptions reported in the *Experimental Section*. As shown in Figures 4A and 4B, the impact of both capital (C_{CAP}, Figure 4A) and operating costs (C_{OP}, Figure 4B) on the production of CO and formate (r_{TOT}) strongly depended on the adopted values of P and j. The impact of C_{CAP}, measured as euros spent for the electrolyser for each mole of CO and formate produced (€ mol_{TOT}^{-1}), under adopted operative conditions, strongly decreased with j (Figure 4A) due to the higher productivities achieved at the highest js (Figure 3B). In particular, at 40 bar,

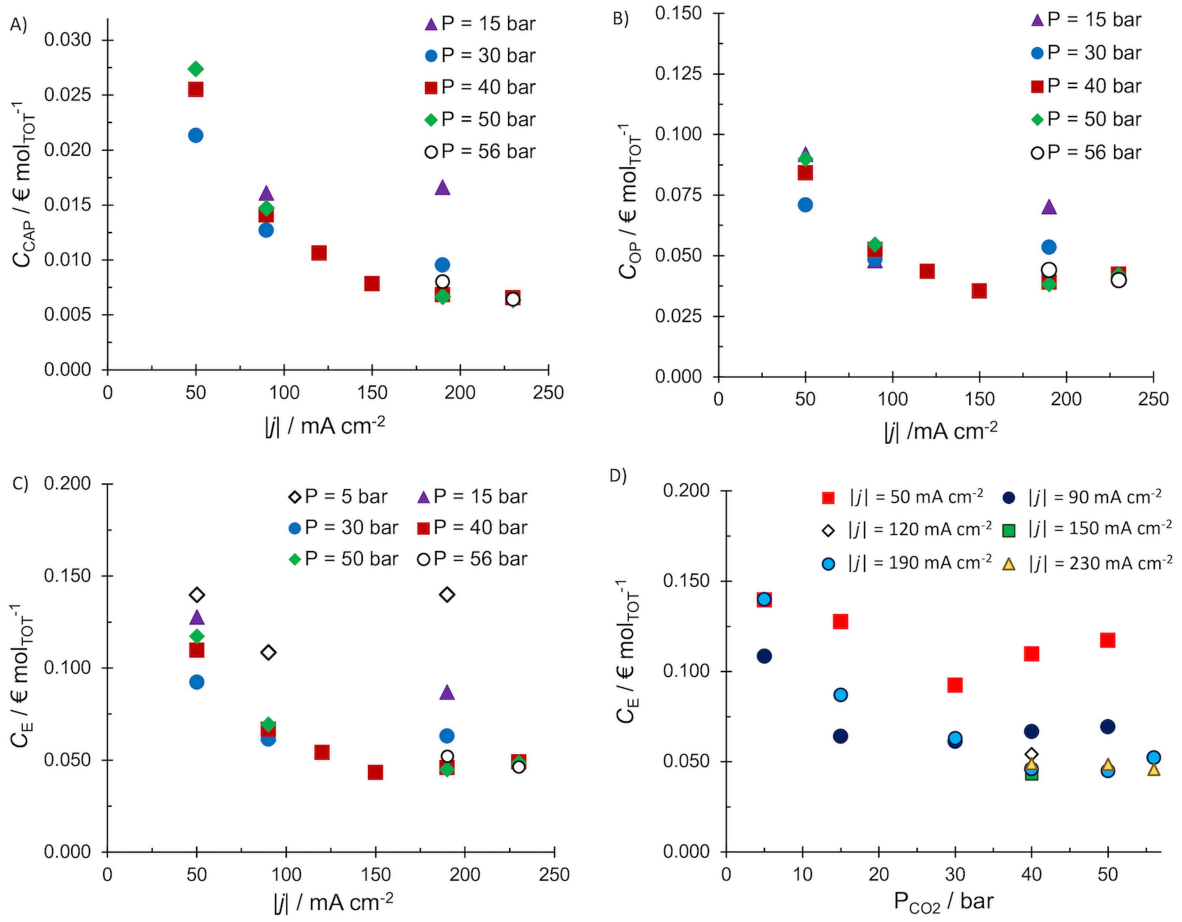

Figure 4. Plot of the (A) C_{CAP}, (B) C_{OP} and (C) C_E vs. j at different P values. (D) Plot of C_E vs. P at different j values.

the minimum impact of C_{CAP} was observed at $-190\ mA\,cm^{-2}$ ($5.6\ 10^{-3}$ € mol_{TOT}^{-1}) and $-230\ mA\,cm^{-2}$ ($5.3\ 10^{-3}$ € mol_{TOT}^{-1}), in spite of the fact that under these conditions, the FE were not the highest ones (Figure 3A) since very high *r* were obtained under these operative conditions. In particular, at $-190\ mA\,cm^{-2}$, the lowest impacts of C_{CAP} were observed at 40 and 50 bar, e.g., at the P that gave the highest *r* (Figure 3B).

A similar picture was observed for the operating costs (C_{OP}) (Figure 4B), which include both the energetic (C_{ENER}) and the chemicals costs ($C_{CHEMICALS}$) (at least CO_2 feed, water process and supporting electrolyte). According to our estimation, C_{OP} are significantly higher than the C_{CAP} (compare Figures 4A and 4B). This is attributed to the higher expense due to the chemicals needed to feed the electrolyser unit ($C_{CHEMICALS} > C_{ENER}$, see Figures S2A and S2B in Supporting Information). An interesting picture was observed for the costs related to the consumption of energy (C_{ENER}) which are related to both the FEs and the ΔVs. As shown in Figure S2A, they presented a quite slight increase with *j* up to $-150\ mA\,cm^{-2}$; as an example, at 40 bar, they increased from 7.8 10^{-3} to 10 10^{-3} € mol_{TOT}^{-1} upon increasing *j* from −50 to $-150\ mA\,cm^{-2}$ due to the relatively high values of FE_{TOT} achieved under all these conditions (Figure 3A) and to the slight increase of ΔV with *j*. However, upon enhancing *j* to −190 or $-230\ mA\,cm^{-2}$ a very strong increase of C_{ENER} was observed (Figure S2A) because of the very high ΔVs observed under these conditions (see as an example Figure 2E). Figures 4C and 4D report the impact of the sum of capital and operating costs (C_E) on the process for a large set of operative conditions. It is worth to mention that the highest values were achieved at 5 bar (Figures 4C and 4D), because of the low values of FEs and *r*s, thus confirming the opportunity to operate with relatively high P. Relatively low values close to 0.048 € mol_{TOT}^{-1} were obtained for a large set of couples P_{CO2} - *j* using P of 40 and 50 bar (with *j* from −90 to $-190\ mA\,cm^{-2}$) and 15 bar (at *j* of $-90\ mA\,cm^{-2}$). However, the minimum values were recorded at $-150\ mA\,cm^{-2}$ (Figure 4C) which gave quite high FE and *r* and relatively low values of both C_{CAP} (Figure 4A) and C_{OP} (Figure 4B).

2.6. Stability of the $PrCO_2CR$ Process

Electrolysis was performed at $-190\ mA\,cm^{-2}$ and 40 bar for more than 13 hours to evaluate the stability of the $PrCO_2CR$ process. Figure 5 reports the evolution of FE_{CO} with the time. It was observed that the FE_{CO} remains almost constant at approximately 73 ± 4% for more than 13 hours. This data was coupled with an average CO productivity of $7.2\ mmol\,s^{-1}\,cm^{-2}$. Moreover, both the ΔV (6.7 V) and the EC (about $0.50\ kWh\,mol_{CO}^{-1}$) were almost stable with time, showing the good stability of the $PrCO_2CR$ process at high *j* and P.

In addition, the Ag electrode was characterized by SEM and XRD before and after the long-term electrolysis to evaluate the stability of the used electrode material. The morphology of the surface of the electrode was analyzed using a FEG-ESEM microscope (QUANTA 200 by FEI). The electron microscope images were obtained using both the secondary electron detector (SE) (Figure 6A) and the backscattered electron detector (BSED) (Figure 6B).

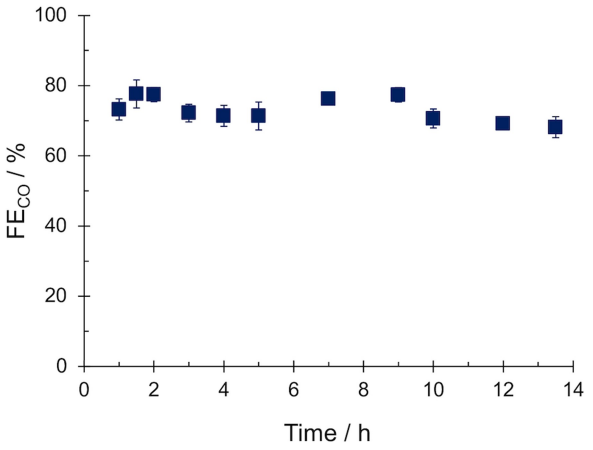

Figure 5. Plot of the FE_{CO} vs time. Electrolyses were performed in a CO_2-saturated 0.5 M $KHCO_3$ aqueous electrolyte using Ag cathode and DSA anode for 13.5 hours at $-190\ mA\,cm^{-2}$ and 40 bar. V = 0.05 L. N = 500 rpm. $Q = 0.1\ L\ min^{-1}$.

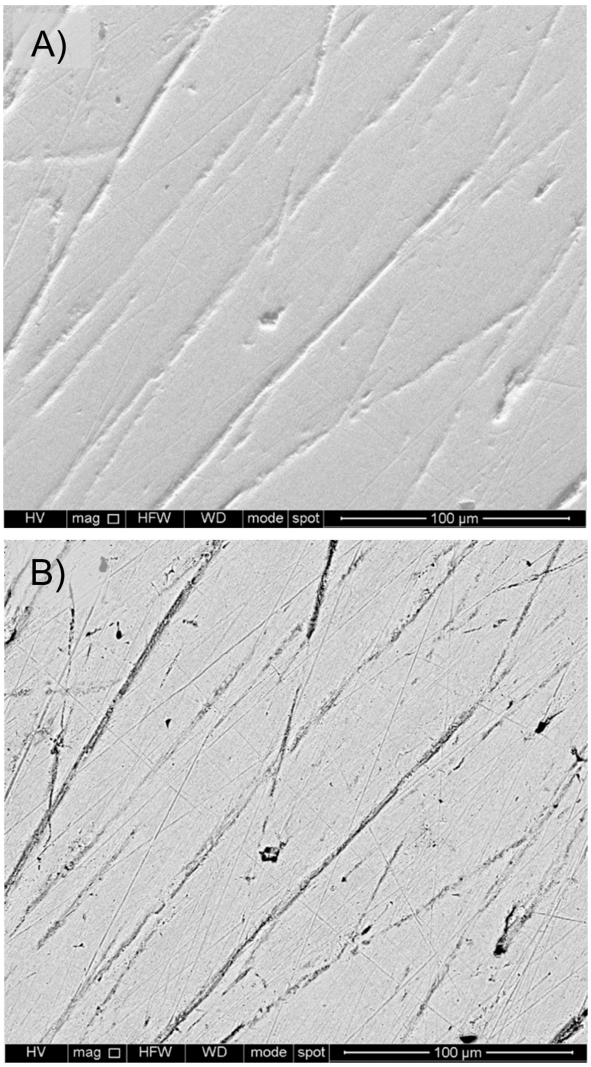

Figure 6. Electron microscope images: A) SE and B) BSED of the Ag cathodes after the long-term electrolysis performed for 13.5 hours at $-190\ mA\,cm^{-2}$ and 40 bar.

The BSED was used to better highlight the morphology of the surface and the possible presence of impurities. The two images show that the surface of the electrode is clean and without deposits. Only the lines due to the cleaning treatment done by abrasion with alumina paste are present. The two images are perfectly mirrored because at BSED the deeper areas appear darker (Figure 6B).

The crystallinity and purity of the electrode were evaluated by X-ray diffraction using a RIGAKU X-ray diffractometer (D-MAX 25600 HK). The XRD pattern of the electrode before the test shows the presence of some diffraction peaks all attributable to the polycrystalline Ag (Figure 7). The peaks were indexed using the card n. 4–783 of the International Centre of Diffraction Database which is related to the face-centered cubic structure of metallic silver. Throughout the width at half height of the main peak, located at approximately 38.45°, and using Scherrer's formula, the mean grains size was calculated finding a value of 27 ± 3 nm. In addition to the silver diffraction peak, no other peaks are present and consequently, it can be concluded that the electrode consists of pure poly-crystalline silver. In the pattern after the test, no differences were detected (Figure 7).

Overall, the morphological analyses, carried out under the electron microscope, and the XRD analysis led to the conclusion that the surface of the electrode did not undergo any modification during the test.

3. Conclusions

The electrochemical conversion of pressurized CO_2 was investigated to explore in a systematic way the effect of the P and of the *j* on the figures of merit of the process. It was found for Ag cathode that:

- the use of relatively high P (40 and 50 bar) allowed to achieve quite high faradic efficiency for a very large interval of *j* up to $-190\ mA\,cm^{-2}$; hence the productivity increased with *j*;
- the plot faradic efficiency vs. P_{CO2} gives a curve with a maximum for all the tested *j*;
- both the P and the *j* strongly affect the selectivity of the cathodic reduction of CO_2, even if in an opposite way: the increase of the P and the decrease of *j* leads to a decrease of formate production with respect to that in CO.

Moreover, it was found that the impact of capital costs decreased upon increasing *j*, due to the high productivities, while the energetic costs are relatively low using *j*s up to $-150\ mA\,cm^{-2}$. Eventually, relatively low values of the the sum of capital and energetic costs are obtained at various values of the couple P_{CO2} - *j* (as an example at $-90\ mA\,cm^{-2}$ from 15 to 50 bar and at $-190\ mA\,cm^{-2}$ at 40 and 50 bar), while the highest values were achieved at the lowest *j* and at the lowest and the highest adopted P_{CO2}.

Experimental Section

Electrochemical Apparatus

A home-made reactor that can work at high-pressure previously described in detail in ref. [17] was used for the experimental trials. A schematic view of the electrochemical high-pressure cell is showed in Figure 8. Briefly, this reactor is made in AISI316 stainless steel and characterized by a cylindrical geometry. The electrolyte (V = 0.05 L) was placed inside the reactor using a pyrex glass container. On the top of the reactor, there is a conax connection for four lines: two for the electrodes, one for the thermocouple, and one of the gas outlet stream. The reactor is fed and pressurized using 5.0 purity CO_2 supplied by Rivoira. Pressure is measured by a pressure gauge of high precision (0.25%). A Ti/IrO_2-Ta_2O_5 sheet, commonly known with a commercial name DSA® supplied by ElectroCell AB was used as counter electrode with a working area of 2.4 cm^2. A plate of silver (Ag, Carlo Erba) with an active surface of 2.4 cm^2 was used as working electrode. The reactor was not equipped with a reference electrode; hence a two-electrode configuration was used setting the reference on the counter. The distance between the electrodes was at 1.7 cm. A magnetic stirrer is used to stir the electrolyte solution during the experiments at a 500 rpm.

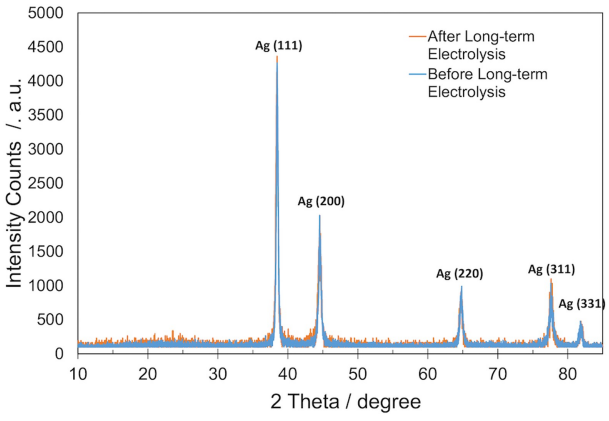

Figure 7. XRD pattern of plate Ag cathode before (orange line) and after (blue light line) the long-term electrolysis performed for 13.5 hours at $-190\ mA\,cm^{-2}$ and 40 bar.

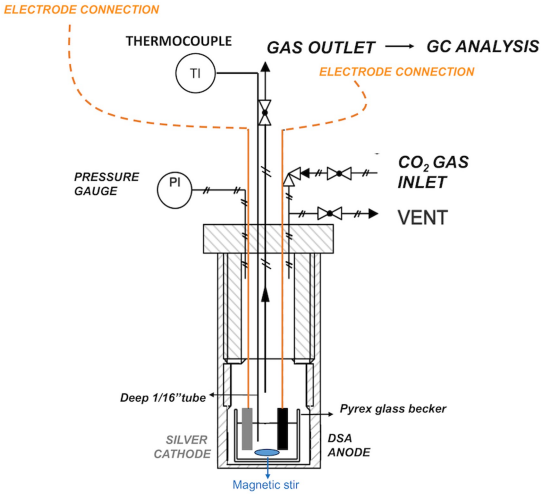

Figure 8. Schematic view of the high-pressure electrochemical cell.

Electrolysis and Analyses

An Amel potentiostat/galvanostat instruments (2053 model) was used to perform the experiments under negative galvanostatic condition (j from -50 to -230 mA cm^{-2}). Electrolyses were performed with saturated CO_2 aqueous electrolyte of $KHCO_3$ (0.5 M) at different pressure values ranged between 1 and 56 bar. Before each electrolysis, the Ag electrode was polished with an alumina powder suspension (size 1 μm), sonicated in HPLC grade water for 5 min, and then rinsed with HPLC grade water. DSA® was cleaned by an ultrasound bath for 5 minutes. Autolab PG STAT12 Methrom was used to carry out chronoamperometric curves in a wide range of pressure and current density. The area of the working electrode for chronoamperometric curves was fixed at 0.1 cm^2. Formic acid and formate [FA] were evaluated by Agilent HP 1100 HPLC using a Rezex-ROA-Organic Acid H+ (8%) column. Analyses were carried out with an UV detector at a wavelength of 210 nm. 0.005 N H_2SO_4 aqueous solution with pH 2.5 was eluted at 0.5 mL min^{-1} as mobile phase. The analysis was performed at 20 °C. Under the adopted operative condition, the retention time of FA was 18 minutes. CO, CO_2, H_2 and other possible gas products were quantified using an Agilent 7890B GC equipped with a thermal conductivity detector (TCD) at 230 °C. A Supelco Carboxen® 60/80 column was used. Helium (99.999%, supplied by Air Liquide) as carrier gas was used at 1 bar. Column temperature was *i*) at 35 °C for 5 min *ii*) followed by a 20 °C min^{-1} ramp up to 225 °C and *iii*) by an isothermal step at 225 °C for 40 min.

The performances of the process were evaluated considering the figures of merit:

- faradic efficiency of CO, FA and H_2 ($FE_{CO,}$ FE_{FA} and FE_{H2}) and the FE_{CO2_TOT} defined by Eq.s (7), (8), (9)and (10):

$$FE_{CO} = z^*F^*[CO]^*Q/I^*100\ [=]\ \% \tag{7}$$

$$FE_{FA} = z^*F^*[FA]^*V/(I^*t)^*100\ [=]\ \% \tag{8}$$

$$FE_{H2} = z^*F^*[H2]^*Q/I^*100\ [=]\ \% \tag{9}$$

$$FE_{CO2\_TOT} = FE_{CO} + FE_{FA}\ [=]\ \% \tag{10}$$

Where z is the electrons exchanged number ($z=2$ in all cases of CO, FA and H_2), F the Faraday constant (96485 C mol^{-1}), [CO], [FA] and [H2] the concentration of CO, FA and H_2, respectively (mol m^{-3} and mol L^{-1} in the case of FA and CO, respectively), Q the volumetric flow rate (m^3 s^{-1}), V (L) electrolyte volume, and I the current intensity (A);

- the productivity r_i defined by Eq. (11):

$$r_i = FE_i/100^*j/z\ F\ [=]\ \text{mmol s}^{-1}\ \text{m}^{-2} \tag{11}$$

where i is CO, FA or TOT and refers to produced mole of CO, FA or the total moles, respectively.

- the selectivity of the process toward CO (Eq. (12)):

$$S_{CO} = FE_{CO}/FE_{CO2\_TOT}{}^*100\ [=]\ \% \tag{12}$$

Energy consumption (EC) (Eq. (13)):

$$EC = \Delta V^*I^*t/\text{mol}_i\ [=]\ \text{kWh mol}^{-1} \tag{13}$$

where ΔV is the cell potential, and mol_i the amount of CO, FA or total moles obtained (mol).

Each experiment was replicated three times. Average data were provided in the manuscript. In most of cases data were reproducible with an error lower than 6%.

The crystal structure was analyzed by X-ray analysis using a RIGAKU diffractometer (model: D-MAX 25600 HK). Diffraction spectra were acquired in the 2θ range from 10 to 85°. The morphology was examined by a QUANTA 200 FEI field emission gun (FEG) Environmental Scanning Electron Microscope (ESEM).

Economic Analysis

Here, the economic analysis includes the main costs correlated to capital and energetic costs for the electrolysis process. The total electrolysis costs (C_E) were estimated by the sum of the capital (C_{CAP}) and operation (C_{OP}) costs and expressed as the € per mole of CO and FA produced (€ mol_{TOT}^{-1}). These costs were estimated by taking into consideration that, currently, the available CO_2CR technologies are not ready to be implemented at the applicative scale since they are still in the development stage (TRL = 3–5), and there is no available data in the literature for the stability of the process.[1,5,48] According to these considerations, the assessment costs involve some degree of uncertainty. The capital costs (C_{CAP} [=] € mol_{TOT}^{-1}) were computed by considering an electrolyzer of an active area of 1 m^2, 20 years as plant lifetime and 8000 hours per years of operation. The price of the undivided electrochemical cell (P_{Cell}) was estimated of 15410 € m^{-2} in line with Cañizares et al.[49] For the pressure factors, cell manufacturing cost and piping cost are not influenced ranging the operative pressure between 1 and 20 bar.[12] Moreover, commercial cell and industrial tube are able to work up to 20 bar. Hence, an additional pressure factor of 22 or 47% of the P_{Cell} was considered by working at pressure lower or higher than 23 bar, respectively. Electrode cost was assumed of approximately 6000 € m^{-2} according to the market value of an Ag foil with a thickness of 0.1 mm, 99,99% high purity silver sheet supplied by Hebei Zanzhen Welding Material Co. Ltd, China. Recently, in their review, Fernández-Caso et al.[48] highlighted that a cathode lifetime over 4.45 yr (close to 40000 h) would neglect both the influence of the cathode fabrication from an environmental perspective and keep the influence of the consumable cost in the total cost of production below 10%. Hence, in our estimation, we assume the cathode lifetime of 40000 h. The operation cost (C_{OP}) was estimated taking into consideration the energetic costs and the main chemicals used in the process. The energetic costs (C_{ENER}) were computed taking into account the electrolysis unit energy consumption (EC) and for the CO_2 gas stream compression at the different operative pressure (P_a) (Eq. (14)) (it was observed that they are less than the 2% of the total energy required). Hence, here the power consumption for a given capacity (kWh mol_{TOT}^{-1}) was estimated by Eq. (15)

$$P_a = F_v{}^*P_{atm}\ \gamma/(\gamma\text{-}1)\ [(P/P_{atm})^{(\gamma-1)/\gamma}\text{-}1]/\eta/\text{mol}_{TOT}\ [=]\ \text{kW mol}_{TOT}{}^{-1.} \tag{14}$$

$$C_{ENER} = (EC + P_a)^*P_E \tag{15}$$

Where F_v is the flow of the make-up of CO_2 (m^3 s^{-1}), P and P_{atm} the operative pressure and the atmospheric one, respectively, γ the compressibility factor of CO_2 of 1.3, the efficiency η was assumed of 50%, P_E is the electricity price (€ kWh^{-1}) (0.03 € kWh^{-1}[8]). The other operation costs, namely chemicals costs ($C_{CHEMICALS}$), were related to the CO_2 capture and recycling costs, water process and supporting electrolyte. According to ref. [12], in the first approximation approach, it was assumed that pure CO_2 was fed to the electrolyzer at a capture cost of 34 € t_{CO2}^{-1} (i.e. 0.00149 € mol_{CO2}^{-1}). In the

current literature, the CO_2 conversion per pass for the current electrochemical technologies is drastically lower than 100%. Hence, unreacted CO_2 needs to be recirculated; the lower the CO_2 conversion, the higher the separation costs of gaseous by-products in the CO_2 recycled stream. CO_2 recycling cost was estimated as the 80% of the CO_2 capture costs according to ref. [21]. The water process cost was assumed 1.30 € m^{-3} according to ref. [13]. It was assumed that 80% of the water process was recycled to the electrolysis unit.[21] The supporting electrolyte $KHCO_3$ prices was fixed at 0.46 € kg^{-1} according to potassium bicarbonate at 99% grade price CAS N 298-14-6 supplied by Jiangsu Coroge Health Technology Co., Ltd. It was assumed that 80% of the supporting electrolyte salt could be recycled since during the separation process (e.g. distillation) for the concentration and separation stage of the liquid product stream an oversaturation of $KHCO_3$ in water is expected[21] and part of the salt can be recovered.

Acknowledgements

University of Palermo is acknowledged for its finantial support. Open Access publishing facilitated by Università degli Studi di Palermo, as part of the Wiley - CRUI-CARE agreement.

Conflict of Interests

The authors declare no conflict of interest.

Data Availability Statement

The data that support the findings of this study are available from the corresponding author upon reasonable request.

Keywords: electrochemistry · reduction · CO_2 conversion · high-pressure · CO

[1] R. I. Masel, Z. Liu, H. Yang, J. J. Kaczur, D. Carrillo, S. Ren, D. Salvatore, C. P. Berlinguette, *Nat. Nanotechnol.* **2021**, *16*, 118–128.
[2] W. Zhang, Y. Hu, L. Ma, G. Zhu, Y. Wang, X. Xue, *Adv. Sci.* **2018**, *5*, 1700275.
[3] O. S. Bushuyev, P. De Luna, C. T. Dinh, L. Tao, G. Saur, J. Van De Lagemaat, S. O. Kelley, E. H. Sargent, *Joule* **2018**, *2*, 825–832.
[4] P. R. Yaashikaa, P. S. Kumar, S. J. Varjani, A. Saravanan, *J. CO_2 Util.* **2019**, *33*, 131–147.
[5] F. Proietto, U. Patel, A. Galia, O. Scialdone, *Electrochim. Acta* **2021**, *389*, 138753.
[6] M. F. Philips, G. J. M. Gutter, M. T. M. Koper, K. J. P. Schouten, *ACS Sustainable Chem. Eng.* **2020**, *8*, 15430–15444.
[7] C. Tang, P. Gong, T. Xiao, Z. Sun, *Nat. Commun.* **2021**, *12*, 2139.
[8] H. Zhang, S. Zeng, C. Jiang, K. Peng, J. Feng, L. Yuan, X. Li, F. Xu, X. Zhang, *ChemCatChem* **2024**, e202400045.
[9] S. Yang, M. Jiang, M. Wang, L. Wang, X. Song, Y. Wang, Z. Tie, Z. Jin, *Nano Res.* **2023**, *16*, 8910–8918.
[10] B. F. Snyder, M. Layne, D. E. Dismukes, *Int. J. Greenhouse Gas Control* **2020**, *93*, 102885.
[11] Z. Huang, R. G. Grim, J. A. Schaidle, L. Tao, *Energy Environ. Sci.* **2021**, *14*, 3664–3678.
[12] F. Proietto, A. Galia, O. Scialdone, *ChemElectroChem* **2021**, *8*, 2169–2179.
[13] M. Jouny, W. Luc, F. Jiao, *Ind. Eng. Chem. Res.* **2018**, *57*, 2165–2177.
[14] H. Krassig, J. Schurz, R. G. Steadman, K. Schliefer, W. Albrecht, M. Mohring, H. Schlosser, in *Ullmann's encyclopedia of industrial chemistry*, Wiley-VCH, **2012**, *6*, 679–693.
[15] V. Subramani, S. K. Gangwal, *Energy Fuels* **2008**, *22*, 814–839.
[16] J. Li, J. Guo, H. Dai, *Sci. Adv.* **2022**, *8*, eabo0399.
[17] F. Proietto, R. Rinicella, A. Galia, B. Avila-Bolívar, V. Montiel, J. Solla-Gullón, O. Scialdone, *J. Environ. Chem. Eng.* **2023**, *11*, 109903.
[18] F. Proietto, F. Berche, A. Galia, O. Scialdone, *J. Appl. Electrochem.* **2021**, *51*, 267–282.
[19] C. M. Gabardo, A. Seifitokaldani, J. P. Edwards, C.-T. Dinh, T. Burdyny, M. G. Kibria, C. P. O'Brien, E. H. Sargent, D. Sinton, *Energy Environ. Sci.* **2018**, *11*, 2531–2539.
[20] E. J. Dufek, T. E. Lister, S. G. Stone, M. E. McIlwain, *J. Electrochem. Soc.* **2012**, *159*, F514–F517.
[21] M. Ramdin, A. R. T. Morrison, M. de Groen, R. van Haperen, R. de Kler, L. J. P. van den Broeke, J. P. M. Trusler, W. de Jong, T. J. H. Vlugt, *Ind. Eng. Chem. Res.* **2019**, *58*, 1834–1847.
[22] A. Kudo, S. Nakagawa, A. Tsuneto, T. Sakata, *J. Electrochem. Soc.* **1993**, *140*, 1541–1545.
[23] K. Hara, A. Tsuneto, A. Kudo, T. Sakata, *J. Electrochem. Soc.* **1994**, *141*, 2097–2103.
[24] M. Todoroki, K. Hara, A. Kudo, T. Sakata, *J. Electroanal. Chem.* **1995**, *394*, 199–203.
[25] K. Hara, A. Kudo, T. Sakata, *J. Electrochem. Soc.* **1995**, *391*, 141–147.
[26] O. Scialdone, A. Galia, G. Lo Nero, F. Proietto, S. Sabatino, B. Schiavo, *Electrochim. Acta* **2016**, *199*, 332–341.
[27] F. Proietto, R. Rinicella, A. Galia, O. Scialdone, *J. CO_2 Util.* **2023**, *67*, 102338.
[28] F. Proietto, B. Schiavo, A. Galia, O. Scialdone, *Electrochim. Acta* **2018**, *277*, 30–40.
[29] S. Siahrostami, A. Moshar, M. M. Farmand, *Fresenius Environ. Bull.* **2003**, *12*, 1202–1206.
[30] T. Mizuno, K. Ohta, A. Sasaki, T. Akai, M. Hirano, A. Kawabe, *Energy Sources* **1995**, *17*, 503–508.
[31] F. Köleli, D. Balun, *Appl. Cataly. A-Gen.* **2004**, *274*, 237–242.
[32] L. Huang, G. Gao, C. Yang, X.-Y. Li, R. K. Miao, Y. Xue, K. Xie, P. Ou, C. T. Yavuz, Y. Han, G. Magnotti, D. Sinton, E. H. Sargent, W. Lu, *Nat. Commun.* **2023**, *14*, 2958.
[33] J. Li, Y. Kuang, Y. Meng, X. Tian, W.-H. Hung, X. Zhang, A. Li, M. Xu, W. Zhou, C.-S. Ku, C.-Y. Chiang, G. Zhu, J. Guo, X. Sun, H. Dai, *J. Am. Chem. Soc.* **2020**, *142*, 7276–7282.
[34] F. Proietto, S. Li, A. Loria, X.-M. Hu, A. Galia, M. Ceccato, K. Daasbjerg, O. Scialdone, *J. Chem. Eng.* **2022**, *49*, 132251.
[35] L. Huang, G. Gao, C. Yang, X.-Y. Li, R. K. Miao, K. X. Xue, P. Ou, C. T. Yavuz, Y. Han, G. Magnotti, D. Sinton, E. H. Sargent, X. Lu, *Nat. Commun.* **2023**, *14*, 2958.
[36] S. Lamaison, D. Wakerley, J. Blanchard, D. Montero, G. Rousse, D. Mercier, P. Marcus, D. Taverna, D. Giaume, V. Mougel, M. Fontecave, *Joule* **2020**, *4*, 395–406.
[37] H. Hashiba, S. Yotsuhashi, M. Deguchi, Y. Yamada, *ACS Comb. Sci.* **2016**, *18*, 203–208.
[38] N. Girichandran, S. Saedy, R. Kortlever, *Chem. Eng. J.* **2024**, *487*, 150478.
[39] A. R. T. Morrison, V. van Beusekom, M. Ramdin, L. J. P. van den Broeke, T. J. H. Vlugt, W. de Jong, *J. Electrochem. Soc.* **2019**, *166*, E77–E86.
[40] F. Proietto, A. Galia, O. Scialdone, *ChemElectroChem* **2019**, *6*, 162–172.
[41] X. Li, C. Peng, J. P. Crawshaw, G. C. Maitland, J. P. M. Trusler, *Fluid Phase Equilib.* **2018**, *458*, 253–263.
[42] B. Kim, S. Ma, H.-R. M. Jhong, P. J. A. Kenis, *Electrochim. Acta* **2015**, *166*, 271–276.
[43] X.-G. Zhang, X. J. Jin, D.-Y. Wu, Z.-Q. Tian, *J. Phys. Chem. C* **2018**, *122*(44), 25447–25455.
[44] X. Zhu, J. Huang, M. Eikerling *ACS Catal.* **2021**, *11*, 14521–14532.
[45] W. Zhang, Z. Jin, Z. Chen, *Adv. Sci.* **2022**, *9*, 2105204.
[46] W. Zhang, C. Xu, Y. Hu, S. Yang, L. Ma, L. Wang, P. Zhao, C. Wang, J. Ma, Z. Jin, *Nano Energy* **2020**, *73*, 104796.
[47] H. Zhong, K. Fujii, Y. Nakano, *J. Electrochem. Soc.* **2017**, *164*, F923–F927.
[48] K. Fernández-Caso, G. Díaz-Sainz, M. Alvarez-Guerra, A. Irabien, *ACS Energy Lett.* **2023**, *8*(4), 1992–2024.
[49] P. Cañizares, R. Paz, C. Sáez, M. A. Rodrigo, *J. Environ. Manage.* **2009**, *90*, 410–420.

Manuscript received: March 8, 2024
Revised manuscript received: May 6, 2024
Accepted manuscript online: May 7, 2024
Version of record online: June 7, 2024